Acceleration of the Antarctic Circumpolar Current by Wind Stress along the Coast of Antarctica

JAN D. ZIKA

University of Southampton, and National Oceanography Centre, Southampton, United Kingdom

JULIEN LE SOMMER

CNRS, LGGE, and University of Grenoble Alpes, Grenoble, France

CAROLINA O. DUFOUR*

University of Grenoble Alpes/CNRS/INPG, LEGI, Grenoble, France

ALBERTO NAVEIRA-GARABATO

University of Southampton, and National Oceanography Centre, Southampton, United Kingdom

ADAM BLAKER

National Oceanography Centre, Southampton, United Kingdom

(Manuscript received 8 April 2013, in final form 12 August 2013)

ABSTRACT

The influence of wind forcing on variability of the Antarctic Circumpolar Current (ACC) is investigated using a series of eddy-permitting ocean–sea ice models. At interannual and decadal time scales the ACC transport is sensitive to both the mean strength of westerly winds along the ACC circumpolar path, consistent with zonal momentum balance theories, and sensitive to the wind stresses along the coast of Antarctica, consistent with the ''free mode'' theory of Hughes et al. A linear combination of the two factors explains differences in ACC transport across 11 regional quasi-equilibrium experiments. Repeated single-year global experiments show that the ACC can be robustly accelerated by both processes. Across an ensemble of simulations with realistic forcing over the second half of the twentieth century, interannual ACC transport variability owing to the free-mode mechanism exceeds that due to the zonal momentum balance mechanism by a factor of between 3.5 and 5 to one. While the ACC transport may not accelerate significantly owing to projected increases in along-ACC winds in future decades, significant changes in transport could still occur because of changes in the stress along the coast of Antarctica.

1. Introduction: The ACC

The Antarctic Circumpolar Current (ACC) is the largest current in the World Ocean. The ACC links the three major ocean basins along its path around Antarctica (Gordon 2001). Its consequent steeply sloping isopycnals connect a huge fraction of the deep ocean to the atmosphere (Rintoul et al. 2001; Johnson and Bryden 1989). Turbulent processes, themselves intimately linked to the ACC, play a major role in exchanges between near-surface waters and the ocean interior (Marshall 1997; Zika et al. 2013). Knowledge of what drives the ACC is thus critical to our understanding of ocean circulation and climate.

Simple models of the ACC present a linear relationship between its transport and the strength of the winds in the Southern Hemisphere (e.g., Marshall and Radko 2003; Allison et al. 2010). Although realistic ocean

* Current affiliation: Atmospheric and Ocean Sciences, Princeton University, Princeton, New Jersey.

Corresponding author address: Jan D. Zika, University of Southampton, National Oceanography Centre, Empress Dock, Southampton, SO143ZH, United Kingdom.
E-mail: J.D.Zika@soton.ac.uk

DOI: 10.1175/JPO-D-13-091.1

models show some relationship between the winds and the ACC transport, the story is far more complex (Gnanadesikan and Hallberg 2000; Gent et al. 2001; Tansley and Marshall 2001).

In addition to wind strength, modeled ACC transport is known to be influenced by thermodynamics (Gnanadesikan and Hallberg 2000; Gent et al. 2001), the parameterization of mixing processes (Gent et al. 2001), the explicit resolution of eddies (Hallberg and Gnanadesikan 2006), and intrinsic processes related to eddy–mean flow interactions (Hogg and Blundell 2006; Hughes et al. 1999). Each of these affects the variability of the ACC on different time scales (Olbers and Lettmann 2007; Webb and de Cuevas 2007). Promisingly, however, it is likely that on interannual time scales the forcing, in particular the wind forcing, is dominant in controlling the ACC transport (Treguier et al. 2010). The control of the ACC by wind forcing on interannual to decadal time scales is the topic of the present study.

Proposed mechanisms for wind-forced variability of the ACC are discussed in section 2. The eddy-permitting ocean models employed in this study are described in section 3. We show that the ACC transport can be strongly influenced by both the strength of the wind stress along the ACC and the strength of the wind along f/H contours along the coast of Antarctica in quasi-steady experiments (section 4) and perturbation experiments (section 5). The interannual variability from a range of models forced by different atmospheric products is discussed in section 6. The major conclusions of this study are then summarized in section 8.

2. Two driving mechanisms of ACC transport variability

Here, two mechanisms are discussed by which wind forcing can influence the strength of the ACC: zonal momentum balance and free-mode acceleration.

a. Zonal momentum balance

Consider an ocean with a free surface elevation η, depth H, depth-integrated velocity $\mathbf{U}$, pressure p, and external stress $\boldsymbol{\tau}$. The depth-integrated momentum equation may be written [following Hughes and de Cuevas (2001)]

$$\rho_0 \mathbf{U}_t + \rho_0 f \mathbf{k} \times \mathbf{U} = -\int_{-H}^{\eta} \nabla p \, dz + \boldsymbol{\tau} + \mathbf{B}. \qquad (1)$$

In (1), ρ_0 is the density of seawater, $\mathbf{U}_t$ is the time derivative of $\mathbf{U}$, f is the Coriolis frequency, $\mathbf{k}$ is the unit vector in the vertical (z), and $\mathbf{B}$ is the depth integral of the viscous stress divergence and nonlinear and fluctuating terms in $\mathbf{U}$. Zonally integrating (1) in realistic dynamically steady ocean models, Hughes and de Cuevas (2001) show that the dominant balance is between the pressure gradient term and the zonal wind stress τ_x term such that

$$\oint \int_{-H}^{\eta} \frac{\partial p}{\partial x} dz \, dx \approx \oint \tau_x \, dx. \qquad (2)$$

The lhs of (2) represents topographic form stress and can be interpreted as the stress placed on the solid earth by the ocean. In this interpretation, the zonal momentum imparted by the wind stress (right-hand side) is removed at the sea floor by form stress (left-hand side). The implication of (2) for the zonal mean volume transport is that the equatorward Ekman transport (right-hand side) is balanced by a poleward geostrophic flow (left-hand side).

As the Southern Ocean is unbounded at the latitudes of Drake Passage (from approximately 60° to 54°S, Fig. 1) the momentum balance implies that the wind stress can only be extracted by bottom form stress below the sill depth (~2000 m). Thus, the equatorward Ekman transport is balanced only below the sill depth by the return geostrophic flow. Acting on a stably stratified ocean, this zonally averaged meridional overturning tilts isopycnals, leading to an acceleration of the ACC (Johnson and Bryden 1989).

Although it is thought that the zonal momentum balance mechanism contributes to setting the mean ACC transport (Gent et al. 2001), it is unclear what role it has in setting interannual to decadal variability. Coarse-resolution climate models with rudimentary eddy parameterizations tend to display a linear relationship between wind strength along the ACC and ACC transport (Allison et al. 2010) when all other forcing factors remain fixed. However, it has been suggested that increased wind forcing will result in increased vertical momentum transfer by mesoscale eddies and hence will not result in increases in ACC transport, a mechanism dubbed ''eddy saturation'' (Straub 1993; Hogg and Blundell 2006).

b. Free-mode acceleration

An alternative mechanism for the wind-forced variability of the ACC is developed from a barotropic viewpoint. Dividing (1) by H and taking its curl, one arrives at the following depth-integrated vorticity equation:

$$\rho_0 \nabla \cdot \left(\frac{\nabla \Psi_t}{H} \right) + \rho_0 J(\Psi, f/H) = \rho_0 J(E, 1/H) + \mathbf{k} \cdot \nabla \times \frac{\boldsymbol{\tau}}{H} + \mathbf{k} \cdot \nabla \times \frac{\mathbf{B}}{H}, \qquad (3)$$

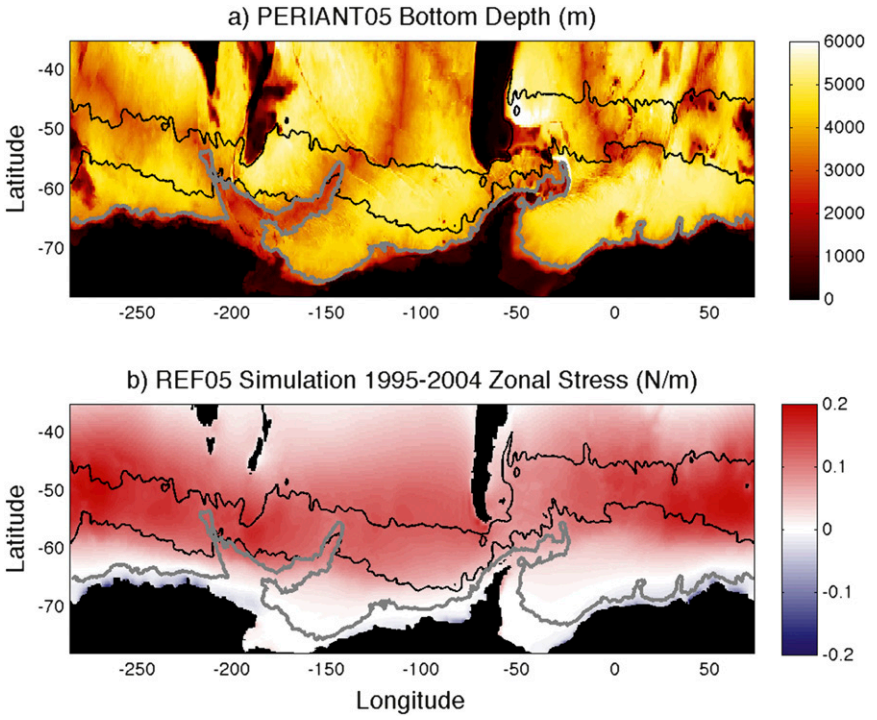

FIG. 1. (a) PERIANT05 bottom depth and (b) REF05 mean surface stress. Shown are the northern (20 Sv) and southern (132 Sv) streamlines of the Antarctic Circumpolar Current in REF05 (black contours) and the $f/H = -4 \times 10^{-8}\,\mathrm{s}^{-1}\,\mathrm{m}^{-1}$ contour (gray line).

where Ψ is the depth-integrated streamfunction, Ψ_t is its temporal derivative, and E is the potential energy defined by

$$E = g \int_{-H}^{\eta} \rho z \, dz \tag{4}$$

in which g is gravitational acceleration. Integrating (3) along a circumpolar contour of constant f/H with along contour length elements $d\mathbf{s}$ and neglecting $\mathbf{B}$ and the potential energy term one arrives at

$$\rho_0 \oint_{f/H} \frac{\mathbf{k} \times \nabla \Psi_t}{H} \cdot d\mathbf{s} \approx \oint_{f/h} \frac{\boldsymbol{\tau}}{H} \cdot d\mathbf{s}. \tag{5}$$

Here, (5) implies that along an f/H contour the depth-averaged velocity is accelerated by surface stress. In the absence of friction ($\mathbf{B}$) and changes in the potential energy

$$\left[\frac{\partial}{\partial t} J(E, 1/H) \approx 0\right]$$

the flow can continue unhindered along an f/H contour. This phenomenon is known as a "free mode" (Read et al. 1986).

Hughes et al. (1999) proposed that a free mode could exist around Antarctica and the free-mode mechanism could control variability of the ACC. Hughes et al. found strong correlations between the ACC transport of the (eddy permitting) Fine Resolution Antarctic Model (FRAM) (The FRAM group 1991) and wind stress fluctuations along closed f/H contours around Antarctica (e.g., where $f/H = -4 \times 10^{-8}\,\mathrm{s}^{-1}\,\mathrm{m}^{-1}$, Fig. 1) at up to annual time scales. Analysis of a simplified ocean model by Olbers and Lettmann (2007) has suggested that the free-mode mechanism may, indeed, influence variability on decadal and longer time scales.

In this study, we will use realistic eddy-permitting ocean models to test whether the ACC transport is sensitive to changes in wind forcing along the ACC and along f/H contours around Antarctica on interannual to multidecadal time scales.

3. Ocean models

We make use of two coupled ocean–sea ice configurations of the Nucleus for European Ocean Modelling (NEMO) (Madec 2008): the regional Southern Ocean configuration PERIANT05 and the global configuration ORCA025. Quasi-steady experiments are carried out using PERIANT05 and repeated single-year experiments

are carried out using a configuration of ORCA025 with different wind perturbations. Furthermore an ensemble of five multidecadal ORCA025 hindcast experiments are analyzed with different initial conditions and internal parameters. All simulations use the Louvain-la-Neuve Ice Model, version 2 (LIM2) (Timmerman et al. 2005).

PERIANT05 is a configuration of the entire ocean south of 30°S. The resolution is 0.5° (cosine latitude) giving a grid size of approximately 28 km at 60°S (roughly equivalent to FRAM). The reference simulation will hereafter be referred to as REF05 (the full name is PERIANT05–GCDMP5 in the Drakkar model archive). REF05 is forced at the sea surface by Drakkar Forcing Set 3 (DFS3) (Brodeau et al. 2010) [a composite of 40-yr European Centre for Medium-Range Weather Forecasts (ECMWF) Re-Analysis (ERA-40) and ECMWF products] and at 30°S by the output of the simulation ORCA05–G70.112 (Drakkar-Group 2007; Barnier et al. 2006). Simulations are initialized from rest and with the National Oceanographic Data Center World Ocean Atlas (Levitus and Boyer 1994) and run from 1980 to 2004. To avoid spurious trends in ACC transport due to the misrepresentation of bottom water in this specific configuration [a ubiquitous problem in eddy-permitting z-coordinate models as discussed by Lee et al. (2002)], we restore temperature and salinity in the deepest layers in REF05 to climatological values with a 2-yr restoring time scale. REF05 is described in greater detail in Dufour et al. (2012). This restoration is not applied to the ORCA025 experiments described below.

All diagnostics performed on PERIANT05 are averages taken over the last 10 years of the 25-yr experiments. As Dufour et al. (2012) show, the model has reached a quasi-equilibrium in terms of ACC transport by the 15th year.

ORCA025 is a 0.25° (cosine latitude) global configuration giving an approximate grid size of 14 km at 60°S. In the simulations used in this study ORCA025 has a bi-Laplacian horizontal eddy viscosity of $1.5 \times 10^{11}\,\mathrm{m^4\,s^{-2}}$, a vertical viscosity of $10^{-4}\,\mathrm{m^2\,s^{-1}}$, and employs a turbulent eddy kinetic energy closure and a background vertical mixing coefficient of $10^{-5}\,\mathrm{m^2\,s^{-1}}$.

We will make specific use of the simulations CORE025–1, CORE025–2, and CORE025–NY. CORE025–1 is a hindcast experiment run from rest from 1958 to 2007 using reanalysis forcing from the second Coordinated Ocean Reference Experiment (CORE2; Large and Yeager 2009). CORE025–2 is started from the output of CORE025–1 in 2007 and run from 1989 to 2007, using identical forcing. [Original names for the CORE025–1 and CORE025–2 experiments are ORC025–N206 and ORCA025–VN206, respectively, and these are also described in Blaker et al. (2013, manuscript submitted to *Climate Dyn.*).] CORE025–NY is started from the output of CORE025–2 in 2004 and run for 16 years (from 2004 + 1 to 2004 + 16) using CORE2 "normal-year forcing" (NY) repeated each year. Repeated single-year wind perturbations are carried out for years 2004 + 10 and 2004 + 11. These are discussed in section 5.

An additional set of ORCA025 hindcast experiments are also analyzed in section 6. The additional experiments are DFS025–L46, DFS025–1, and DFS025–2, which are also discussed in Treguier et al. (2010). Each experiment is forced by DFS3, the same forcing used in the PERIANT05 simulations. Differences between the ORCA025 simulations and relevant references are listed in Table 1. No deep restoring is applied in the ORCA025 experiments, and as a consequence some simulations do have a significant drift in their ACC transport (Treguier et al. 2010).

The models employed in this project have been widely validated by users within the Drakkar community (Drakkar-Group 2007; Barnier et al. 2006). In terms of their performance in the Southern Ocean, the PERIANT05 simulations have been discussed by Dufour et al. (2012) and the ORCA025 experiments by Treguier et al. (2007) and (2010). In particular the ability of equivalent ORCA025 experiments to reproduce observed global patterns of interannual sea level anomaly (SLA) variability, including that driven by intrinsic processes, is unprecedented (Penduff et al. 2011).

4. PERIANT05 quasi-steady experiments

We will now use PERIANT05 to explore the role of wind forcing in setting the decadal to longer-term variability of the ACC. This is done by running the model to quasi equilibrium over 25 years with constant changes made to the reference forcing.

Dufour et al. (2012) ran PERIANT05 with a series of mean changes in the wind forcing. The simulations include WIND05+, WIND05++, and WIND05+++ where the magnitude of the winds is increased by 10%, 20%, and 30%, respectively, and SAM05+, SAM05++, and SAM05+++ where a wind pattern is added to the forcing, consistent with a half, one, and two standard deviations of the southern annular mode (SAM), respectively.

Here we discuss additional experiments to those of Dufour et al. (2012), where stress under sea ice is modified. In the simulations described in Dufour et al. and each of the ORCA025 experiments, stress imparted from the sea ice onto the ocean surface is attenuated with an exponential decay function. An additional set of experiments has been run and is presented here in which there is no attenuation. As such, a larger fraction of the momentum imparted by the winds on the sea ice is transferred from the sea ice to the ocean. The net effect of this is that the

TABLE 1. Summary of attributes of the PERIANT05 and ORCA025 simulations. Where simulation names are given in the initial conditions column, final output of the simulation is used as the initial condition of the new experiment, with the exception of NY–WIND025 and NY–ANT025 where the outputs of CORE025–NY are used at the end of years +9 and +10. DFS: Drakkar Forcing Set and CORE: Coordinated Ocean Reference Experiment; $\mathbf{u}_{\mathrm{Air}}$ is the 10-m atmospheric wind, and $\tau_{\mathrm{Ice-Ocean}}$ is the stress between the ice and ocean.

Run	Levels	Forcing	Period	Initial conditons	Reference
PERIANT05 0.5° cos(lat) regional expts (ocean south of 30°S)					
REF05	46	Reanalysis (DFS3)	1980–2004	Climatology	Dufour et al. (2012)
WIND05	46	Increased wind ($\lvert\mathbf{u}_{\mathrm{Air}}\rvert$)	1980–2004	Climatology	Dufour et al. (2012)
SAM05	46	Increased SAM	1980–2004	Climatology	Dufour et al. (2012)
ICE–REF05	46	Increased $\lvert\boldsymbol{\tau}_{\mathrm{Ice-Ocean}}\rvert$	1980–2004	Climatology	This study
ICE–WIND05	46	Incr. $\lvert\mathbf{u}_{\mathrm{Air}}\rvert$ and $\lvert\boldsymbol{\tau}_{\mathrm{Ice-Ocean}}\rvert$	1980–2004	Climatology	This study
ORCA025 0.25°cos(lat) global ocean expts					
DFS025–L46	46	Reanalysis (DFS3)	1958–2004	Climatology	Barnier et al. (2006)
DFS025–1	75	Reanalysis (DFS3)	1958–2001	Climatology	Treguier et al. (2010)
DFS025–2	75	Reanalysis (DFS3)	1958–2001	DFS025–1	Treguier et al. (2010)
CORE025–1	75	Reanalysis (CORE2)	1958–2007	Climatology	Blaker et al. (2013, manuscript submitted to *Climate Dyn.*)
CORE025–2	75	Reanalysis (CORE2)	1989–2007	CORE025–1	Blaker et al. (2013, manuscript submitted to *Climate Dyn.*)
CORE025–NY	75	Normal year (CORE2)	from +1 to +16	CORE025–2	This study
NY–WIND025	75	Increased westerlies	+10 and +11	CORE025–NY	This study
NY–ANT025	75	Reduced easterlies	+10 and +11	CORE025–NY	This study

westward stress felt by the ocean along the coast of Antarctica is increased (i.e., more westward stress) as is the easterly stress felt by the ocean in the seasonal sea ice zones farther north. Both the sea ice formulation used by Dufour et al. and all ORCA025 experiments presented here and the sea ice formulation used in the ICE–REF05 and ICE–WIND05 experiments are described in detail in the appendix.

The effect of the different ice stress formulations results in increased westward stress along the coast of Antarctica in ICE–REF05, as compared to REF05, as the prevailing wind is westward there (see the appendix). Four experiments are run with this formulation: ICE–REF05 otherwise identical to REF05 and ICE–WIND05+, ICE–WIND05++ and ICE–WIND05+++ otherwise identical to WIND05+, WIND05++, and WIND05+++, respectively.

Following Allison et al. (2010), we compute the mean stress along the mean path of the ACC (Fig. 2a) as indicated by the mean depth-integrated streamfunction ψ (defined by cumulatively integrating the zonal transport from the south). In each simulation, the along ACC wind stress τ_{ACC} is defined as the area-averaged zonal wind stress between a southern streamline ψ_S and a northern streamline ψ_N such that

$$\tau_{\mathrm{ACC}} = \frac{\oint\int \prod(\psi - \psi_S) \prod(\psi_N - \psi)\tau_x \, dx \, dy}{\oint\int \prod(\psi - \psi_S) \prod(\psi_N - \psi) \, dx \, dy}. \quad (6)$$

Above Π is a unit step function or Heaviside function [$\Pi(x) = 0$ for $x < 0$ and $\Pi(x) = 1$ for $x \geq 0$], τ_x is the zonal surface stress component, and integrals are taken over the entire domain. The southern streamline $\psi_S = 20$ Sv (i.e., 20 Sv from the coast of Antarctica) and $\psi_N = \psi(55°\mathrm{S}, 67°\mathrm{W}) - 20$ Sv (i.e., 20 Sv from the Americas; $1\ \mathrm{Sv} \equiv 10^6\ \mathrm{m^3\ s^{-1}}$). Streamlines ψ_S and ψ_N are shown in Fig. 2a. The same streamlines are used for all the PERIANT05 simulations (i.e., the streamlines do not change location from simulation to simulation).

As Dufour et al. (2012) recognize, both SAM05++ and WIND05+++ wind patterns tend to increase their ACC transport, as measured through Drake Passage by approximately 12 and 16 Sv, respectively. They point out that the wind pattern in SAM05++ accelerates the ACC more strongly than the pattern in WIND05+++, despite WIND05+++ having a greater along-ACC stress. In the ICE–REF05 and ICE–WIND05 experiments, the ACC transport is smaller than in the REF05 and WIND05 experiments by 8–12 Sv despite very little change in τ_{ACC} (Fig. 2a).

To assess whether the wind stress along f/H contours has a role in setting the ACC transport, we average the zonal ocean stress along the $f/H = -4 \times 10^{-8}\ \mathrm{s^{-1}\ m^{-1}}$ contour (gray contour in Fig. 1; Hughes et al. 1999) defining

$$\tau_{f/H} = \oint_{f/H} \boldsymbol{\tau} \cdot d\mathbf{s} \Big/ \oint_{f/H} |ds|, \quad (7)$$

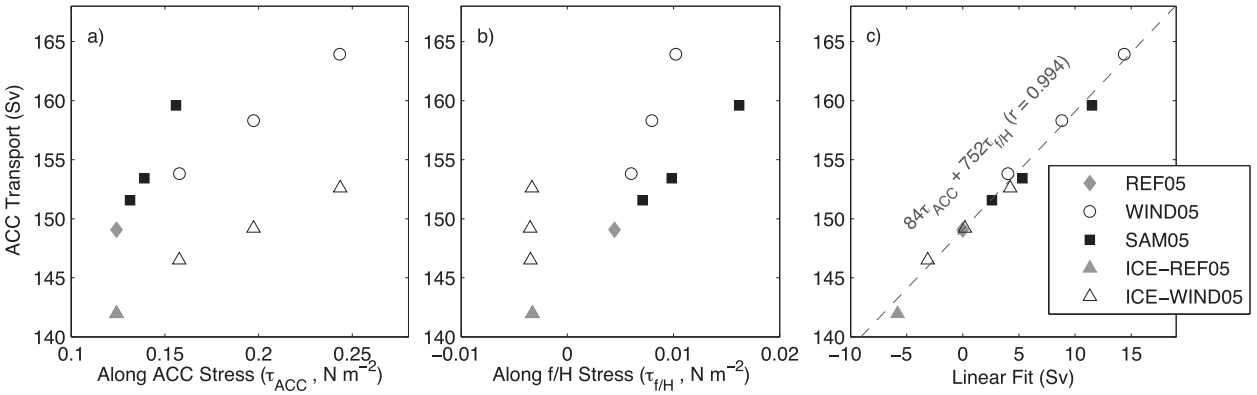

FIG. 2. (a) Zonal wind stress along the ACC (averaged between the black lines in Fig. 1) vs ACC transport in the PERIANT05 experiments, (b) mean wind stress along $f/H = -4 \times 10^{-8}\,\mathrm{s^{-1}\,m^{-1}}$, and (c) ACC transport vs a least-squares fit assuming the transport anomaly is a linear function of both along-ACC wind stress and along-f/H stress.

where $d\mathbf{s}$ are the directional length elements (positive in the cyclonic direction), and $|ds|$ are the absolute length elements along the f/H contour. We choose the $f/H = -4 \times 10^{-8}\,\mathrm{s^{-1}}$ contour as this was recognized by Hughes et al. (1999) as the contour along which winds were most highly correlated with wind stress.

We have also used an alternative definition for the along-f/H stress $\tau^{\mathrm{Zonal}}_{f/H}$, defined as the average zonal stress at points closest to Antarctica where $f/H > -4 \times 10^{-8}\,\mathrm{s^{-1}\,m^{-1}}$ at each longitude. This gives a contour that simply hugs the coast of Antarctica (i.e., does not deviate to the north in the western South Pacific). Although correlations between $\tau_{f/H}$ and the ACC transport are always larger than correlations between $\tau^{\mathrm{Zonal}}_{f/H}$ and the ACC transport, all conclusions made in this study are qualitatively robust using either definition. This suggests also that the particular choice of f/H contour does not greatly influence the results presented here.

In the REF05, WIND05, and SAM05 experiments $\tau_{f/H}$ is positive (eastward), meaning that this component of the winds is acting to accelerate the ACC via the free-mode mechanism. In the ICE–REF05 and ICE–WIND05 experiments $\tau_{f/H}$ is negative (westward), implying that the wind should decelerate the ACC via the free-mode mechanism (Fig. 2b).

Simulations where $\tau_{f/H}$ is held approximately constant (e.g., WIND05) show linear increases in ACC transport with increasing τ_{ACC}. Likewise, experiments where τ_{ACC} is held constant (e.g., REF05 and ICE–REF05) show increasing ACC transport with increasing $\tau_{f/H}$. We thus ask whether a linear combination of τ_{ACC} and $\tau_{f/H}$ can explain the transport (T_{ACC}) variability between the experiments using the following formula:

$$T'_{\mathrm{ACC}} = a_1 T'_{\mathrm{ACC}} + a_2 \tau'_{f/H}, \tag{8}$$

where the prime represents a deviation from the mean of all the experiments and a_1 and a_2 are unknown constants. A least-squares regression over all PERIANT05 model simulations results in $a_1 = 84\,\mathrm{Sv\,(N\,m^{-2})^{-1}}$ and $a_2 = 752\,\mathrm{Sv\,(N\,m^{-2})^{-1}}$, and the fit has an r value of 0.994 (Fig. 2c). The simulations discussed here are consistent with both the stress along the ACC and along f/H contours around Antarctica contributing to variations in the ACC transport.

In the following section we will undertake annual experiments with a global eddy-permitting model and confirm that both stress variations along the ACC and along f/H contours can accelerate the ACC, and these are significant at interannual time scales.

5. ORCA025 normal-year experiments

Here, we describe the normal-year perturbation experiments carried out using ORCA025. The combination of ORCA025 runs CORE025–1 (1958–2007), CORE025–2 (1989–2004), and CORE025–NY (from 2004 + 1 to 2004 + 16) yields 92 years of continuous simulation. The ACC transport in the CORE runs starts at approximately 160 Sv in 1958 and reaches an apparent equilibrium of 130 Sv during years from 2004 + 1 to 2004 + 16 (Fig. 3).

At interannual time scales, the standard deviation of the linearly detrended ACC transport of CORE025–1 over the period 1970–2007 is 2.5 Sv, while the standard deviation of CORE025–NY is 1.2 Sv. The ACC transport variability of the normal year–forced run CORE025–NY relative to that of the hindcast run CORE025–1 suggests a significant fraction of the variability in CORE025–1 is set by intrinsic processes and this limits the ultimate predictability of the ACC transport in terms of surface stress effects.

Two wind patterns are constructed to specifically assess the role of along-ACC and along-f/H wind stress in

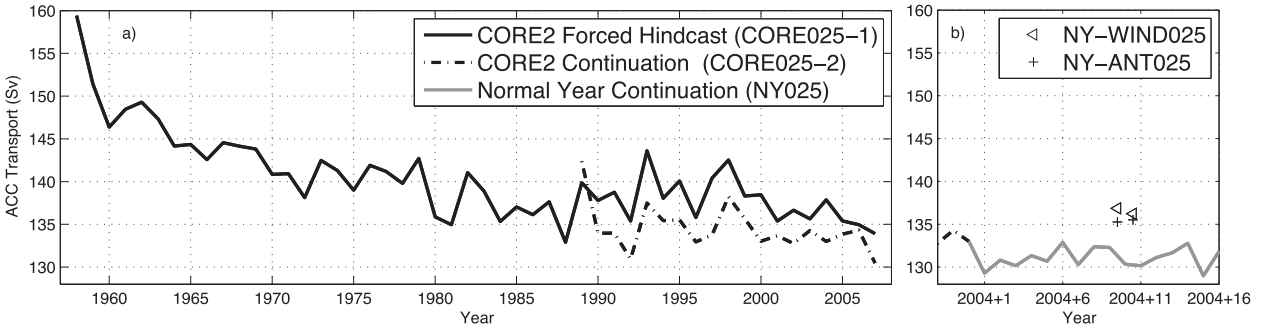

FIG. 3. ACC transport. (a) Simulation CORE025–1 run from rest in 1958–2007 (black solid line), continued into experiment CORE025–2 from 1989 to 2007 (black dot–dashed line). (b) From 2004, CORE025–2 is continued as CORE025–NY using normal year with repeated normal-year forcing for 16 years (from 2004 + 1 to 2004 + 16, gray solid line). Shown are perturbation experiments NY–WIND025 (for years 2004 + 10 and 2004 + 11, triangles) and NY–ANT025 for years 2004 + 10 and 2004 + 11, plus signs).

setting the ACC transport: NY–WIND025 and NY–ANT025. The wind patterns are added to the normal-year forcing to form a yearlong perturbed-forcing time series. The NY–WIND025 pattern is the eastward part of the mean zonal winds in the CORE2 normal-year forcing between 68° and 30°S multiplied by 0.3 (Fig. 4a). This results in a near-parabolic wind anomaly along the mean path of the ACC. The NY–ANT025 anomaly is the westward part of the mean zonal winds south of 40°S multiplied by −1. This results in the mean westward winds along the coast of Antarctica being effectively turned off.

Two experiments are run by adding a wind perturbation to the forcing for one year beginning on 13 August of the 10th normal year (2004 + 10) resulting in experiments NY–WIND025–2004 + 10 and NY–ANT025–2004 + 10. (This date was chosen purely because of the availability of model restart files.) To test the robustness

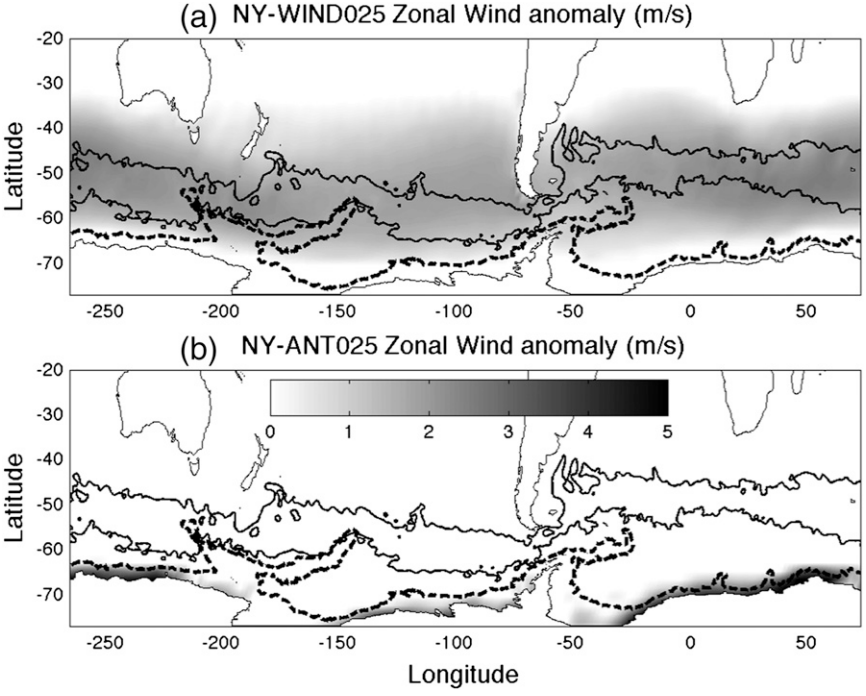

FIG. 4. Zonal 10-m wind anomaly applied in (a) the NY–WIND025 experiments derived as 30% of the mean eastward wind and (b) experiment NY–ANT025 derived as 100% of the mean westward wind south of 30°S. Shown are the northern (20 Sv) and southern (110 Sv) streamlines of the Antarctic Circumpolar Current (black solid lines) and the $f/H = -4 \times 10^{-8}\,\mathrm{s}^{-1}\,\mathrm{m}^{-1}$ contour (black dashed line).

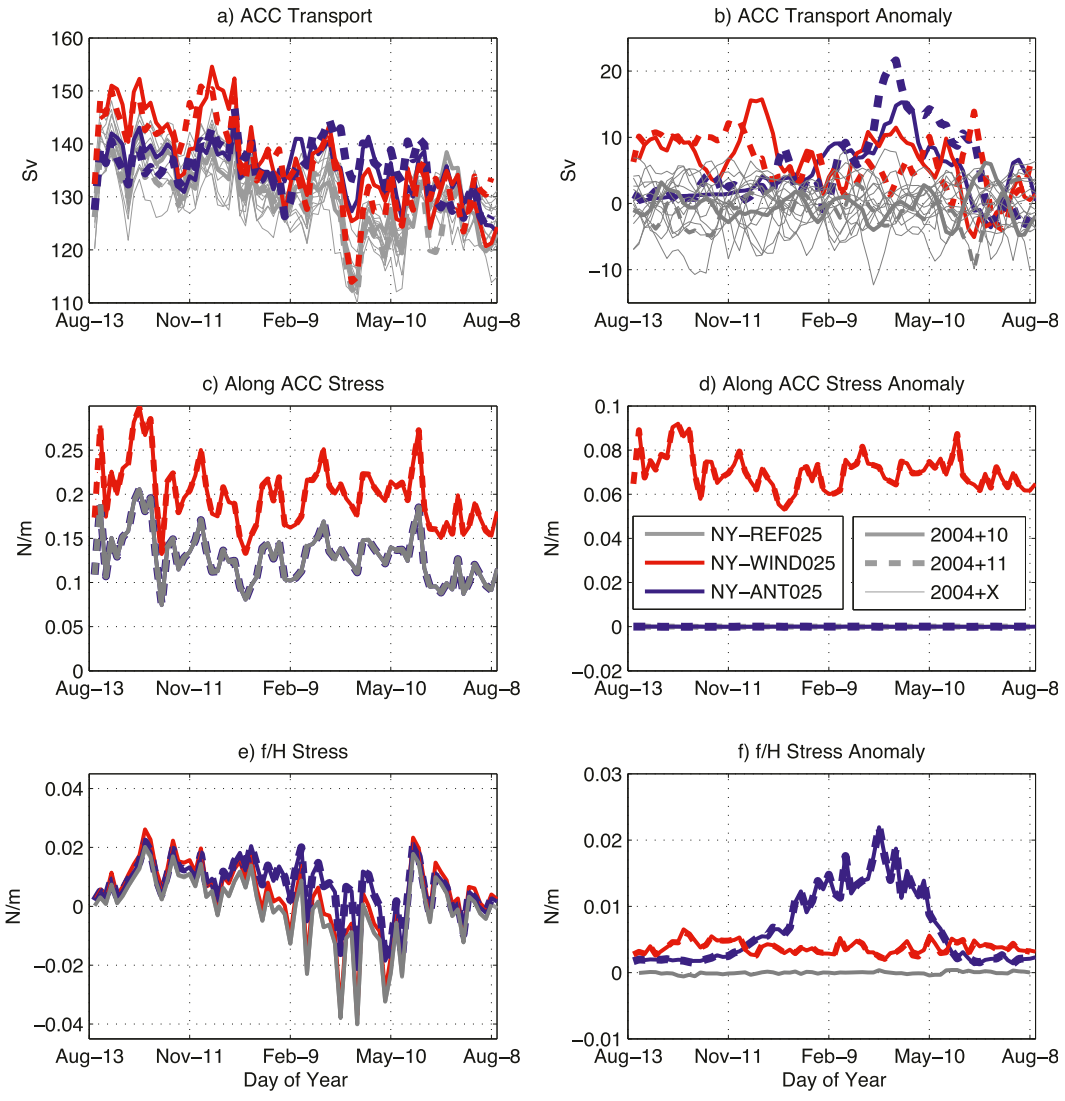

FIG. 5. (a) ACC transport in the normal-year (NY) experiments, (b) ACC transport anomaly (deviation from the mean of all 16 NYs), (c) along-ACC wind stress, (d) along-ACC wind stress anomaly, (e) wind stress along $f/H = -4 \times 10^{-8}\,\mathrm{s}^{-1}\,\mathrm{m}^{-1}$, and (f) f/H stress anomaly. Shown are Expt CORE025–NY for the 10th year after 2004 (2004 + 10, gray solid) and the 11th year after 2004 (2004 + 11, gray dashed), Expt NY–WIND025 (yr +10; red solid), Expt NY–WIND025 (yr +11; red dashed), Expt NY–ANT025 (yr+10; blue solid), and Expt NY–ANT025 (yr+11; blue dashed). Also shown in (a),(b) are years from 2004 + 1 to 2004 + 16 of Expt CORE025–NY (thin gray lines).

of the results to initial conditions and intrinsic processes, two equivalent experiments are carried out beginning on 8 August of the following year (NY–WIND025–2004 + 11 and NY–ANT025–2004 + 11).

In both NY–WIND025–2004 + 10 and NY–WIND025–2004 + 11 experiments, the ACC transport increases by 10 Sv within one month (Figs. 5a,b). The two experiments then decouple, presumably as intrinsic processes take over. The resulting annual average ACC transports are 5.8 Sv and 5.1 Sv above the annual mean of the 16 NY-forced years, respectively. The mean change in wind stress along the ACC is $0.07\,\mathrm{N\,m}^{-2}$.

In the NY–ANT025–2004 + 10 and NY–ANT025–2004 + 11 experiments, the ACC transport increases gradually, peaking late in the austral summer (March–April) at between 15 Sv and 21 Sv above the mean of the normal years. The gradual increase is coincident with the gradual increase in anomalous along $-f/H$ stress in austral summer (Figs. 5e,f). The seasonality of the stress is most likely associated with reduced sea ice cover and the increase in the background wind field amplifying the anomaly ($\boldsymbol{\tau}$ is a polynomial function of the relative wind speed, the appendix). The resulting annual average ACC transports are 4.2 and 4.4 Sv above the annual

mean of the 16 normal years, respectively. The mean change in along-f/H stress is $0.0067\,\mathrm{N\,m^{-2}}$.

There is no change in the along-ACC stress in the NY–ANT025 experiments. Thus, we estimate the linear sensitivity of ACC transport anomaly to $\tau_{f/H}$ [i.e., a_2 in (8)]. We estimate a sensitivity of $a_2 = 620$–$650\,\mathrm{Sv\,(N\,m^{-2})^{-1}}$, comparable yet smaller than the $752\,\mathrm{Sv\,(N\,m^{-2})^{-1}}$ found using PERIANT05.

In the NY–WIND025 experiments, the change in eastward winds does influence the along-f/H stress (Figs. 5e,f red line). Hence both along-ACC and along-f/H stress may be accelerating the ACC in this instance. The implied sensitivity to along-ACC stress is thus $a_1 = 43\,\mathrm{Sv\,(N\,m^{-2})^{-1}}$ [calculated using $a_1 = (T'_{\mathrm{ACC}} - a_2\tau_{f/H})/\tau_{\mathrm{ACC}}$, where $a_2 = 635\,\mathrm{Sv\,(N\,m^{-2})^{-1}}$]. This is significantly smaller than the $84\,\mathrm{Sv\,(N\,m^{-2})^{-1}}$ diagnosed using the quasi-steady PERIANT05 experiments. Note that we do not use the same ACC path for diagnostics of PERIANT05 and ORCA025 data, which, in addition to the change in time scale considered and model horizontal resolution, could explain this difference.

In the following section we quantify how the along-ACC and along-f/H stress varies year-to-year using the output of various models and how much they contribute to the variability of the ACC transport in those models.

6. Interannual variability

We will now compare the interannual variability of the ACC transport with the along-ACC stress and along-f/H stress in the ORCA025 hindcast simulations (Table 1). Anomalies of each quantity are taken from their mean over the whole period and are then detrended (Fig. 6). Correlations between forcing indices and ACC transport are determined for CORE025–1 over the period from 1970 to 2007 and for the mean of DFS025–L46, DFS025–1, and DFS025–2 over the period 1970 to 2001 to allow sufficient model spinup. We do not assess shorter time scales than interannual and we only consider zero-years lag correlations for all indices.

ACC transport variability at interannual time scales is larger in the DFS3-forced simulations (standard deviation = 3.2 Sv) than in the CORE2-forced simulations (standard deviation = 2.5 Sv). The ACC transport in models with the same forcing is well correlated with $r = 0.73$ for CORE025–1 and CORE025–2 (significant at 95% for $r = 0.47$) and $r = 0.88$ for DFS025–1 and DFS025–L46 and $r = 0.9$ for DFS025–2 and DFS025–L46 (significant at 95% for $r = 0.48$). Differences of 1–2 Sv in ACC transport year-to-year between the simulations are expected considering the 1.2 Sv interannual variability of the normal year–forced run (CORE025–NY). Correlations of ACC transport between models with differing forcing is less significant with, for example, $r = 0.44$ for CORE025–1 and DFS025–L46 (significant to 95% for $r = 0.33$).

Along-ACC and along-f/H wind stress is almost perfectly correlated between models with the same forcing and sea ice model (not shown), suggesting that the intrinsic variability in the surface ocean velocity and sea ice cover does not have a major influence on the variability of these indices. Note that we do not change the definition of the ACC path used to determine τ_{ACC} between the different ORCA025 experiments. Between models with different forcing, along-ACC stress is well correlated (CORE025–1 and DFS025–L46; $r = 0.84$) as is the along-f/H stress (CORE025–1 and DFS025–L46; $r = 0.77$).

ACC transport in the CORE2-forced simulations is significantly correlated with both their along-ACC stress (CORE025–1: $r = 0.55$; significant at 95% for $r = 0.32$, CORE025–2: $r = 0.76$) and along-f/H stress (CORE025–1: $r = 0.64$, CORE025–2: $r = 0.67$). In the DFS3-forced simulations, ACC transport is correlated far less significantly with the along-ACC wind stress ($r = 0.38$) than with the along-f/H stress ($r = 0.81$). This is perhaps because the along-ACC wind stress variability is weaker and the along-f/H stress is stronger in the DFS-forced runs than in the CORE-forced runs.

A predicted ACC transport time series is derived for CORE025–1 using (8). Coefficients for the ACC transport change per unit of stress are taken from the NY–WIND025 and NY–ANT025 perturbation experiments [$a_1 = 43\,\mathrm{Sv\,(N\,m^{-2})^{-1}}$ and $a_2 = 635\,\mathrm{Sv\,(N\,m^{-2})^{-1}}$]. Based on (8), the along-ACC wind stress drives variability in CORE025–1 with a standard deviation (SD) of $(a_1\tau_{\mathrm{ACC}}) = 0.4$ Sv and along-f/H stress drives variability of $\mathrm{SD}(a_2\tau_{f/H}) = 1.4$ Sv, with a total of 1.7 Sv predicted by the sum of the two time series (Fig. 7). The sum of the two factors is more correlated with the ACC transport than any one stress diagnostic alone ($r = 0.68$). Applying the same coefficients to data from DFS025–L46, we find that the along-ACC stress is likely to drive variability of SD $(a_1\tau_{\mathrm{ACC}}) = 0.36$ Sv while the along-f/H stress drives $\mathrm{SD}(a_2\tau_{f/H}) = 1.8$ Sv of variability. The ACC transport in DFS025–L46 is less well correlated with that predicted using (8) ($r = 0.78$) than it is with the along-f/H stress alone ($r = 0.81$). A linear fit of (8) to the interannual data from CORE025–1 yields $a_1 = 70\,\mathrm{Sv\,(N\,m^{-2})^{-1}}$ and $a_2 = 539\,\mathrm{Sv\,(N\,m^{-2})^{-1}}$ while for DFS025–L46, $a_1 = -5\,\mathrm{Sv\,(N\,m^{-2})^{-1}}$ and $a_2 = 894\,\mathrm{Sv\,(N\,m^{-2})^{-1}}$.

We have found that the ACC transport is significantly correlated with both along-ACC and along-f/H stress in a range of forced simulations. Given the perturbation experiments carried out and the wind-forced variability from both DFS and CORE, the along-f/H stress is likely

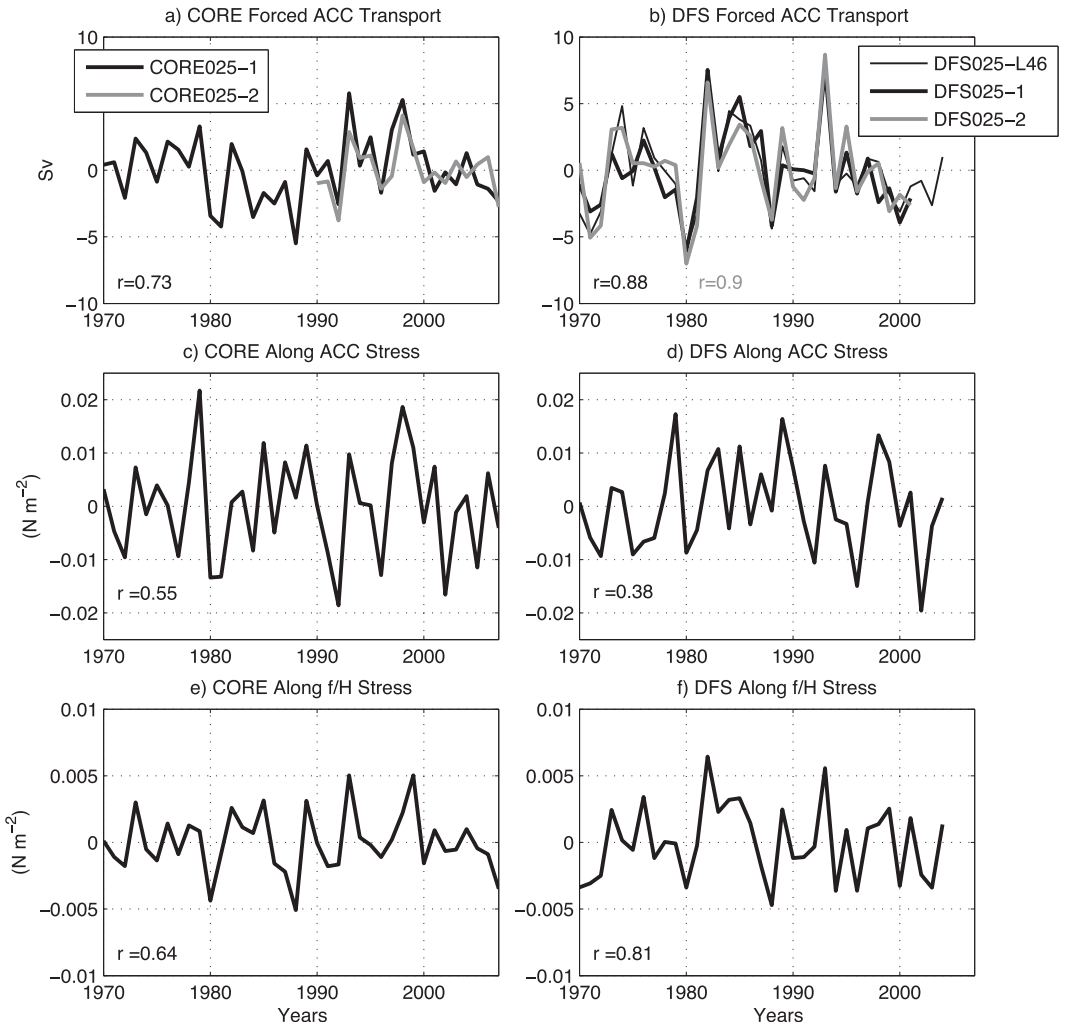

FIG. 6. (a),(c),(e) Results of CORE2-forced simulations CORE025–1 and CORE025–2. (b),(d),(f) Results of DFS3-forced simulations DFS025–L46, DFS025–1, and DFS025–2. ACC transport anomaly is shown in (a),(b); along-ACC wind stress anomaly in (c),(d); and along-f/H stress anomaly in (e),(f). All variables are detrended. Correlation coefficients (r) are shown for correlations with ACC transport; also shown are correlations between the ACC transport of equivalent simulations.

to drive between 3.5 and 5 times as much variability in the ACC as the stress along the ACC [i.e. the ratio of SD ($a_1\tau_{\mathrm{ACC}}$) to SD($a_2\tau_{f/H}$)].

7. Discussion

Recent studies have proposed that the ACC does not vary significantly with changing winds owing to ''eddy saturation'' (Straub 1993; Hogg and Blundell 2006). Such theories suggest that, with increased wind stress along the ACC, mesoscale eddy activity will increase. With this, the rate at which mesoscale eddies flatten isopycnals increases. Hence the ACC transport itself does not need to increase in strength to balance the momentum budget.

In this study, using an eddy-permitting global ocean model (ORCA025), a change in the along-ACC stress of ~50% increases the ACC transport by only 5 Sv over a single year [O(5%) of the total, Figs. 5c,d]. Indeed, the ACC responds by up to 10 Sv on the order of weeks but then decreases over 3–6 months, suggesting a delayed eddy process. Although a comprehensive analysis of the eddy response is left to future work, the lack of acceleration of the ACC may be related to a near eddy saturation or ''effective eddy saturation'', as a perturbation to the mean annual wind stress O(50%) is well outside natural and projected variability. We have found, however, that the free-mode mechanism can effectively drive changes in ACC transport. This suggests that the ACC transport could be, at the same time, insensitive to

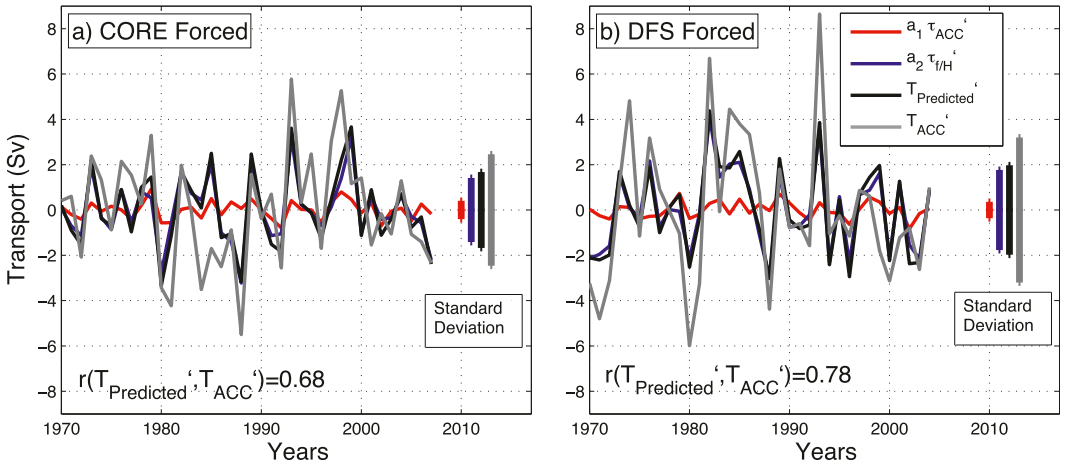

FIG. 7. ACC transport anomaly predicted using (8) with coefficients derived from perturbations experiments NY–WIND025 and NY–ANT025 (black) and the model value (gray): (a) CORE2-forced simulation CORE025–1 and (b) DFS3-forced simulations DFS025–L46. The contribution to the predictions from along ACC stress (τ_{ACC}, red) and along-f/H stress ($\tau_{f/H}$, blue) are also shown along with ± one std dev of each term (vertical bars at right).

changes in along-ACC winds due to eddy saturation, but sensitive to changes in the wind stress along the coast of Antarctica. In which case eddy saturation does not imply the ACC transport will remain constant with changing winds—only that it could remain constant with increased along-ACC winds in the absence of other changes.

Hughes et al. (1999), in proposing the free-mode mechanism for ACC transport variability, also hypothesized that the ACC could be a ''forced free mode.'' A forced free-mode ACC follows f/H contours along much of its circumpolar path and is sensitive to local forcing in isolated regions where such contours are blocked. In such regions wind stress curl can aid or hinder flow across the f/H contour. Mazloff (2012) found that the ACC was, indeed, sensitive to local forcing over regions of intense topographic interaction. It was our initial hypothesis that wind stress curl in the western South Atlantic could accelerate the ACC significantly on annual to decadal time scales in a similar fashion to the forced-free-mode mechanism. Although we still cannot rule out this mechanism, we were unable to generate a wind-forcing pattern whose ACC acceleration could not be explained by either the zonal momentum or free-mode theories.

8. Conclusions

We have demonstrated that the Antarctic Circumpolar Current transport can be influenced by changes in the surface stress both along the ACC, consistent with zonal momentum balance theories, and along the coast of Antarctica, consistent with free-mode theories. Both mechanisms can drive variability on interannual and decadal time scales.

Regional eddy-permitting simulations are performed at 0.5° cos(lat) resolution. Eleven quasi-steady 25-yr simulations are investigated with changes in both wind forcing and ocean–sea ice interactions. These provide a range of ACC transport values for a range of surface stress patterns. The ACC transport anomalies are explained by a linear combination of the stress along streamlines of the ACC and the stress along a continuous f/H contour around Antarctica.

A global 0.25° cos(lat) simulation is run for 68 years with realistic interannually varying forcing, then for a further 16 years with repeating normal-year forcing. Perturbation experiments are performed on the 10th and 11th normal year. Both an anomalous wind stress along the ACC and an anomalous wind stress along f/H contours cause robust increases in ACC transport.

The interannual variability of the ACC transport, along-ACC stress, and along-f/H stress are analyzed for a range of simulations. Both along-ACC and along-f/H stress are significantly correlated with the ACC transport. Based on normal year–perturbation experiments and the observed interannual variability of the surface winds, the free-mode mechanism drives more than 3–5 times greater variability in ACC transport than the zonal momentum balance mechanism.

Acknowledgments. We thank Jean-Marc Molines for his modeling support and Andrew Meijers, Daffyd Gwyn Evans, Andrew McC Hogg, Andrew F. Thompson and Bernard Barnier for comments on versions of this manuscript. This work was supported by the National Environment Research Council through a NERC Fellowship grant and by the Agence Nationale de la Recherche

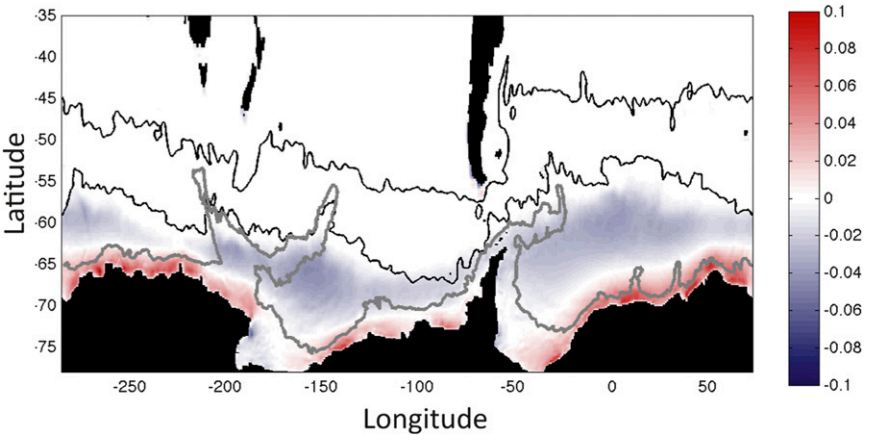

FIG. A1. Mean sea surface stress of ICE–REF05 minus that of REF05. Shown are the northern (20 Sv) and southern (132 Sv) streamlines of the Antarctic Circumpolar Current in REF05 (black contours) and points closest to Antarctica where $f/H = -4 \times 10^{-8}\,\mathrm{s^{-1}\,m^{-1}}$ at each longitude (gray line).

through contract ANR-08-JCJC-0777-01. Julien Le Sommer is supported by the Centre National de la Recherche Scientifique and Carolina Dufour was supported by the French CEA (Commissariat à l'Énergie Atomique). This work used a simulation performed within the frame of the Drakkar project. Drakkar is supported by the Centre National d'Études Spatiales (CNES) through the Ocean Surface Topography Science Team (OST/ST), by the Centre National de la Recherche Scientifique (CNRS), the Institut National des Sciences de l'Univers (INSU) and the Groupe Mission Mercator Coriolis (GMMC).

APPENDIX

Stress under Sea Ice

In all of the simulations discussed here the stress imparted by the wind on the ocean in the absence of sea ice is determined via a conventional bulk formula

$$\boldsymbol{\tau}_{\mathrm{Air\text{–}Ocean}} = \rho_{\mathrm{Air}} C_d |\mathbf{u}_{\mathrm{Air}} - \mathbf{u}_{\mathrm{Ocean}}| (\mathbf{u}_{\mathrm{Air}} - \mathbf{u}_{\mathrm{Ocean}}) \quad \text{(A1)}$$

where ρ_{Air} is the density of air, $\mathbf{u}_{\mathrm{Air}}$ is the wind velocity at 10 m, $\mathbf{u}_{\mathrm{Ocean}}$ is the ocean surface velocity, and C_d is a drag coefficient dependent on the wind speed, atmospheric stability, and temperature and varies between 10^{-3} and 2×10^{-3} (Large and Yeager 2009).

In REF05 (and the ORCA025 experiments) the stress imparted on the ocean by the ice ($\tau_{\mathrm{Ice-Ocean}}$) is

$$\boldsymbol{\tau}_{\mathrm{Ice\text{–}Ocean}} = \rho_0 C_w |\mathbf{u}_{\mathrm{Ice}} - \mathbf{u}_{\mathrm{Ocean}}| (\mathbf{u}_{\mathrm{Ice}} - \mathbf{u}_{\mathrm{Ocean}}) e^{-|\mathbf{u}_{\mathrm{Ice}} - \mathbf{u}_{\mathrm{Ocean}}|/u_0} \quad \text{(A2)}$$

where ρ_0 is the density of seawater, C_w is the ice–ocean drag coefficient, set here to 5×10^3 (Goosse and Fichefet 1999) and $e^{-|\mathbf{u}_{\mathrm{Ice}} - \mathbf{u}_{\mathrm{Ocean}}|/u_0}$ is a function that attenuates the stress when the relative ice–ocean speed is high and where u_0 is an arbitrary constant chosen here to be $0.1\,\mathrm{m\,s^{-1}}$. The total stress felt by the ocean is then

$$\boldsymbol{\tau} = (1 - F_{\mathrm{Ice}}) \boldsymbol{\tau}_{\mathrm{Air\text{–}Ocean}} + F_{\mathrm{Ice}} \boldsymbol{\tau}_{\mathrm{Ice\text{–}Ocean}} \quad \text{(A3)}$$

where F_{Ice} is the fractional ice cover. The mean zonal stress τ_x over the period 1995–2004 in REF05 is shown in Fig. 1b. An additional set of experiments have been run (ICE–REF05, ICE–WIND05+, ICE–WIND05++, and ICE–WIND05+++) where the stress imparted by the ice model into the ocean is not attenuated, so the following equation is used:

$$\boldsymbol{\tau}_{\mathrm{Ice\text{–}Ocean}} = \rho_0 C_w |\mathbf{u}_{\mathrm{Ice}} - \mathbf{u}_{\mathrm{Ocean}}| (\mathbf{u}_{\mathrm{Ice}} - \mathbf{u}_{\mathrm{Ocean}}). \quad \text{(A4)}$$

The difference in $\boldsymbol{\tau}_{\mathrm{Ice-Ocean}}$ between REF05 and ICE–REF05 is shown in Fig. A1.

REFERENCES

Allison, L. C., H. L. Johnson, D. P. Marshall, and D. R. Munday, 2010: Where do winds drive the Antarctic Circumpolar Current? *Geophys. Res. Lett.,* **37,** L12605, doi:10.1029/2010GL043355.

Barnier, B., and Coauthors, 2006: Impact of partial steps and momentum advection schemes in a global ocean circulation model at eddy-permitting resolution. *Ocean Dyn.,* **300,** 543–567.

Brodeau, L., B. Barnier, T. Penduff, and A.-M. Treguier, 2010: An ERA-40-based atmospheric forcing for global ocean circulation models. *Ocean Modell.,* **31,** 88–104.

Drakkar-Group, 2007: Eddy-permitting ocean circulation hindcasts of past decades. *CLIVAR Exchanges,* No. 12, International

CLIVAR Project Office, Southampton, United Kingdom, 8–10.

Dufour, C. O., J. Le Sommer, J. D. Zika, M. Gehlen, J. C. Orr, P. Mathiot, and B. Barnier, 2012: Standing and transient eddies in the response of the Southern Ocean meridional overturning to the southern annular mode. *J. Climate,* **25,** 6958–6974.

Gent, P. R., W. G. Large, and F. O. Bryan, 2001: What sets the mean transport through Drake Passage? *J. Geophys. Res.,* **106** (C2), 2693–2712.

Gnanadesikan, A., and R. W. Hallberg, 2000: On the relationship of the circumpolar current to Southern Hemisphere winds in coarse-resolution ocean models. *J. Phys. Oceanogr.,* **30,** 2013–2033.

Goosse, I., and T. Fichefet, 1999: Importance of ice–ocean interactions for the global ocean circulation: A model study. *J. Geophys. Res.,* **104** (C10), 23 337–23 355.

Gordon, A. L., 2001: Interocean exchange. *Ocean Circulation and Climate,* G. Siedler, J. Church, and J. Gould, Eds., Academic Press, 303–314.

Hallberg, R. W., and A. Gnanadesikan, 2006: The role of eddies in determining the structure and response of the wind-driven Southern Hemisphere overturning: Results from the Modelling Eddies in the Southern Ocean (MESO) project. *J. Phys. Oceanogr.,* **36,** 2232–2251.

Hogg, A. M. C., and J. R. Blundell, 2006: Interdecadal variability of the Southern Ocean. *J. Phys. Oceanogr.,* **36,** 1626–1645.

Hughes, C. W., and B. A. de Cuevas, 2001: Why western boundary currents in realistic oceans are inviscid: A link between form stress and bottom pressure torques. *J. Phys. Oceanogr.,* **31,** 2871–2885.

——, M. P. Meredith, and K. J. Heywood, 1999: Wind-driven transport fluctuations through Drake Passage: A southern mode. *J. Phys. Oceanogr.,* **29,** 1971–1992.

Johnson, G. C., and H. L. Bryden, 1989: On the size of the Antarctic Circumpolar Current. *Deep-Sea Res.,* **36,** 39–53.

Large, W., and S. Yeager, 2009: The global climatology of an interannually varying air–sea flux dataset. *Climate Dyn.,* **33,** 341–364.

Lee, M.-M., A. C. Coward, and A. J. G. Nurser, 2002: Spurious diapycnal mixing of the deep waters in an eddy-permitting global ocean model. *J. Phys. Oceanogr.,* **32,** 1522–1535.

Levitus, S., and T. Boyer, 1994: *Temperature*. Vol. 4, *World Ocean Atlas 1994,* NOAA Atlas NESDIS 4, 117 pp.

Madec, G., 2008: NEMO ocean engine. Institut Pierre-Simon Laplace Note du Pole de modelisation 27, 209 pp.

Marshall, D., 1997: Subduction of water masses in an eddying ocean. *J. Mar. Res.,* **55,** 201–222.

Marshall, J., and T. Radko, 2003: Residual-mean solutions for the Antarctic Circumpolar Current and its associated overturning circulation. *J. Phys. Oceanogr.,* **33,** 2341–2354.

Mazloff, M., 2012: On the sensitivity of the Drake Passage transport to air–sea momentum flux. *J. Climate,* **25,** 2279–2290.

Olbers, D., and K. Lettmann, 2007: Barotropic and baroclinic processes in the transport variability of the Antarctic Circumpolar Current. *Ocean Dyn.,* **57,** 559–578.

Penduff, T., M. E. Juza, B. Barnier, J. D. Zika, W. K. Dewarr, A.-M. Treguier, J.-M. Molines, and N. Audiffren, 2011: Sea level expression of intrinsic and forced ocean variabilities at interannual time scales. *J. Climate,* **24,** 5652–5670.

Read, P., P. Rhines, and A. White, 1986: Geostrophic scatter diagrams and potential vorticity dynamics. *J. Atmos. Sci.,* **43,** 3226–3240.

Rintoul, S. R., C. Hughes, and D. Olbers, 2001: The Antarctic Circumpolar Current system. *Ocean Circulation and Climate,* G. Siedler, J. Church, and J. Gould, Eds., Academic Press, 271–302.

Straub, D., 1993: On the transport and angular momentum balance of channel models of the Antarctic Circumpolar Current. *J. Phys. Oceanogr.,* **13,** 776–782.

Tansley, C. E., and D. P. Marshall, 2001: On the dynamics of wind-driven circumpolar currents. *J. Phys. Oceanogr.,* **31,** 3258–3273.

The FRAM group, 1991: An eddy-resolving model of the Southern Ocean. *Eos, Trans. Amer. Geophys. Union,* **72,** 169–174.

Timmerman, A., H. Goosse, G. Madec, T. Fichefet, C. Ethe, and V. Dulire, 2005: On the representation of high latitude processes in the ORCA-LIM global coupled sea-ice ocean model. *Ocean Modell.,* **8,** 175–201.

Treguier, A.-M., M. England, S. Rintoul, G. Madec, J. Le Sommer, and J.-M. Molines, 2007: Southern Ocean overturning across streamlines in an eddying simulation of the Antarctic Circumpolar Current. *Ocean Sci.,* **3,** 491–507.

——, J. Le Sommer, J.-M. Molines, and B. de Cuevas, 2010: Response of the Southern Ocean to the southern annular mode: Interannual variability and multidecadal trend. *J. Phys. Oceanogr.,* **40,** 1659–1668.

Webb, D. J., and B. A. de Cuevas, 2007: On the fast response of the Southern Ocean to changes in the Zonal wind. *Ocean Sci.,* **3,** 417–427.

Zika, J. D., and Coauthors, 2013: Vertical eddy fluxes in the Southern Ocean. *J. Phys. Oceanogr.,* **43,** 941–955.